Intelligent Initialization and Interactivity: Optimizing Level Sets for T1-weighted White Matter Segmentation

Wenzhe Xue[1], Christine Zwart[2] and Joseph Ross Mitchell[1,2]

[1] Department of Biomedical Informatics, Arizona State University, Scottsdale, AZ 85259, USA,
[2] Department of Radiology, Mayo Clinic, Scottsdale, AZ 85259, USA

Abstract. White matter (WM) segmentation from T1-weighted MRI is complicated by intensity non-uniformities, noise, and WM's high surface area to volume ratio. Accurate algorithms are often computationally intensive and time consuming, precluding interactivity and routine clinical use. To address this we developed a work- and step-efficient parallel narrow-band level set algorithm and mapped this onto commodity GPU hardware. Our algorithm can segment brain WM in 3 seconds. However, it requires expert tuning of 3 parameters. Here we describe recent efforts to improve the precision, accuracy and simplicity of WM segmentation by: a) intelligently initializing algorithm parameters; and, b) allowing interactive parameter tuning during algorithm execution, along with real-time 2D and 3D visualization of parameter effects on segmentation results.

Keywords: Image segmentation, Level set, White matter, User interactive tool, Noise estimation, k-NN, GPU, GPGPU.

1 Introduction

MRI provides high spatial resolution and soft tissue contrast. Consequently, it is widely used for research and clinical neurological studies. Changes in brain morphometry have been linked to childhood development, healthy aging, neurological disorders, and psychiatric disorders. In particular, white matter (WM) develops dramatically through infancy [7] and undergoes significant atrophy as part of healthy aging [6]. WM volume changes can be a very sensitive (if not specific) indicator of Alzheimer's disease and other disorders [8,13].

In the past two decades, a wealth of MR image segmentation algorithms have been developed for automatic or semi-automatic segmentation of WM and other brain structures. Segmentation techniques range from intensity thresholding, to region-based or edge-based methods, to active contour models and level set methods. Despite advances in theoretical approaches, clinics and clinical research laboratories still rely heavily on trained technicians manually delineating regions of interest on each 2D cross-section and then extrapolating to 3D surfaces [2]. The

computation time required for many sophisticated algorithms precludes routine clinical use.

Minimally interactive, user-initiated approaches with manual refinement are often proposed as an ideal solution [2]. Among these algorithms, the level set approach is popular because of its flexibility and robustness [14,11]. The level set (and most region growing) approaches begin with a user-placed seed region of interest (ROI), for example in the WM on the image. The algorithm then iteratively deforms the seed ROI to encompass the entire 'related' area, in our scenario, the entire WM. In addition to the seed region, several algorithm parameters explicitly and intrinsically control the growth and smoothness of the ROI surface. These may include the relative weights of external forces acting on the contour, intensity threshold(s), and a surface smoothness parameter.

Even when the user specification of parameters is well-managed and streamlined (such as in ITK-SNAP [16], a popular semi-automatic segmentation tool), long computation times preclude a truly 'interactive' approach to segmentation. This is particularly true for level sets - the delay between parameter adjustments and outcomes prohibits fine tuning. Approaches to streamline parameter adjustment into a sequential process provides a false sense of fine tuning as the coarse parameters become unavailable baring a fresh start.

A recent work- and step-efficient GPU implementation of the level set method [12] has provided a 14x acceleration over the best previously published GPU approach [10]. A validation study of brain tumor segmentation with the new algorithm showed tumor segmentation times averaging just 1:20 (mm:ss). This was slightly *faster* than diameter-based approaches frequently used in clinical trials, yet provided volume quantification results statistically equivalent to a consensus of manual, slice-by-slice, contour delineations by experts (gold standard) [4]. Furthermore, the speed function used in those studies [12,4] to control the level set surface evolution required specifying only three parameters (intensity window and level and a growth penalty based on surface smoothness). Nevertheless, tuning each parameter to obtain acceptable results required user experience and intuition. Interactive parameter adjustment during algorithm execution, coupled with real time visual feedback of parameter effects on segmentation results, can significantly narrow the intuition gap between novice and experienced users. This is particularly true for high contrast spherical structures (e.g., meningiomas). MRI intensity inhomogeneity, noise, and the complicated surface structure of WM hinders effective parameter selection and, in turn, rapid and accurate brain WM segmentation.

In this paper, we describe a novel approach to initializing the three parameters for GPU level set segmentation of WM in T1 weighted MRI brain images, directly, without user input of specific thresholds or values. Initially, users mark foreground and background seed pixels using a paint-brush style interface. A fuzzy classification model of the seed ROI intensities then controls the local growth and contraction of the level set. Next, we use an empirically determined relationship between curvature, segmentation accuracy, and image noise to predict the optimal curvature influence. Finally, the graphical user interface permits

visualizing the growth of the level set curve as it is computed and permits adjustment of the curvature parameter in real time while observing the surface progression in two or three dimensions. Each of these aspects is reviewed in the Methods (Section 2) prior to coverage of our white matter segmentation results (Section 3) and a brief discussion (Section 4). Videos of our tool and other additional materials have been provided online as well (see Section 5).

2 Methods

2.1 Level Sets

Level set methods embed an implicit surface within an image, and iteratively deform the surface to envelop the ROI. Several comprehensive reviews of level set methods and their application to image segmentation are well-documented in the medical image analysis literature [14]. Here we review the formulation relevant to our algorithm.

The implicitly represented level set surface is defined as $\{\mathbf{x}|\phi(\mathbf{x},t) = 0\}$, where $\mathbf{x}$ is a coordinate in the image volume, t is the current iteration time in the level set evolution, and $\phi(\mathbf{x},t) : \Re^4 \mapsto \Re$ refines the level set according to:

$$\phi(\mathbf{x},t) = \phi(\mathbf{x},t-\Delta t) + \nabla t \cdot F(\mathbf{x},t)|\nabla\phi(\mathbf{x},t-\Delta t)|. \tag{1}$$

A speed function $F(\mathbf{x})$ defines the rate of motion of each local point on the implicit surface. The deforming direction of each point is along the norm of the local surface. Our previous GPU level set algorithm [12] adopted the speed function proposed in [10]:

$$F(\mathbf{x},t) = \alpha C(\mathbf{x},t) + (1-\alpha)D(\mathbf{x}), \tag{2}$$

where $C(\mathbf{x},t)$ is the curvature term, $D(\mathbf{x})$ is the data term, and $\alpha \in [0,1]$, the weight of curvature term, is a blending term that controls the relative contribution of the curvature and data terms.

The data term used in [10] is a function of intensities in a single image volume:

$$D(\mathbf{x}) = \epsilon - |I(\mathbf{x}) - T|, \tag{3}$$

where $I(\mathbf{x})$ is the image intensity at location $\mathbf{x}$, T is a user-specified target intensity that encourages maximum level set growth, and ϵ is a user-specified parameter that indicates the range of intensities around T that will promote level set growth. If $T - \epsilon < I(\mathbf{x}) < T + \epsilon$, then $D(\mathbf{x})$ will promote surface growth. Otherwise it will promote surface contraction.

The curvature term $C(\mathbf{x},t)$ depends upon the mean curvature of the local surface from the previous iteration:

$$C(\mathbf{x},t) = \nabla \cdot \frac{\nabla\phi(\mathbf{x},t-\Delta t)}{|\nabla\phi(\mathbf{x},t-\Delta t)|}. \tag{4}$$

Penalizing curvature prevents critical leakage through weak boundaries and fills holes caused by noise inside the segmented region. Excessive smoothing by overly penalizing curvature (assigning larger value to α) can significantly distort the shape of target objects. Eventually, when α is too large (close to 1), the level set surface will shrink to a point.

The speed function defined by Eq. 2 relies on three user-specified parameters: α, ϵ, and T. T and ϵ define the local intensity force; α defines the contribution of the curvature term. In this paper, we describe a non-parametric approach for specifying the data term, replacing T and ϵ with user seeding of foreground and background pixels. We further suggest an approach to initializing α based on the application (WM segmentation in T1 weighted MR) and image noise, thereby minimizing non-intuitive user input.

2.2 Non-parametric data term

We propose a novel non-parametric data term (in place of Eq. 3) based on the k nearest neighbor (k-NN) algorithm [5]. k-NN algorithms classify objects by assigning the label of majority among the k nearest training samples in feature space. The training data contain samples belonging to either foreground or background. This introduces the added requirement for users to seed both foreground and background voxels. The data term is then defined as a function of relative distance (intensity difference) to the background and foreground classes.

For voxel $\mathbf{x}$ with intensity $I(\mathbf{x})$, the distance to background $d_B(\mathbf{x})$ and distance to foreground $d_F(\mathbf{x})$ samples are assigned as the mean of distances to the k_B and k_F nearest background and foreground samples:

$$d_B(\mathbf{x}) = \frac{1}{k_B} \sum_{k=1}^{k_B} |I(\mathbf{x}) - V_B(k)|; \tag{5}$$

$$d_F(\mathbf{x}) = \frac{1}{k_F} \sum_{k=1}^{k_F} |I(\mathbf{x}) - V_F(k)|. \tag{6}$$

$k_B = \sqrt{N_B}$ and $k_F = \sqrt{N_F}$, where N_B and N_F are the numbers of background and foreground samples respectively. V_B and V_F are sorted feature (intensity) vectors of background and foreground samples.

The new data term is formed based on both distances:

$$D(\mathbf{x}) = \frac{d_B(\mathbf{x}) - d_F(\mathbf{x})}{d_B(\mathbf{x}) + d_F(\mathbf{x})}, \tag{7}$$

and is in the range $[-1, 1]$. Positive values indicate the voxel is closer to the foreground class, and negative values indicate the voxel is closer to the background class. The function is zero-valued when the distances to both classes are equal. Substituting Eq. 7 for Eq. 3 eliminates user-defined parameters T and ϵ.

2.3 Curvature Weighting Term

In Eq. 2, the user-controlled weighting parameter α determines the relative cost of increased curvature. Changes in α over the full theoretical range of values ($\alpha \in (0, 1)$) can significantly impact the segmentation results. For a given application the reasonable range of values for α can be greatly reduced and the initial value for α can be automatically assigned more intelligently than, for example, setting an arbitrary starting point (e.g., $\alpha = 0.5$). This places the user into a fine-tuning and final adjustment role that requires less time, training, and improves the overall algorithm precision. In Section 3.2, we briefly review experiments used to define the optimal starting value for α for based on an empirical relationship between curvature, image noise, and WM segmentation accuracy (Figure 4).

2.4 Software and User Interface

Our tool provides an interactive rendering window with 2D axial or 3D views. Users can quickly switch between 2D and 3D view modes with a shortcut key. In the 3D view, our tool renders the image volume as well as the segmentation results, allowing qualitative validation.

In the first step of the segmentation, users initialize the level set by sketching seed points on axial slices with a paint-brush tool. Users are required to label background samples (out of the targeted ROI) and foreground samples (in the targeted ROI). After pressing the "play" button, the level set iteratively grows to envelop the structures of interest. Due to our unique GPU implementation, both the level set and visualization algorithms share data buffers. This allows interactive tuning of algorithm parameters along with real-time 2D or 3D visualization of the parameter effects on segmentation results. Users can go back to the previous segmentation step using the undo button. In addition, users can manually edit the segmentation results (adding or erasing) using a paint-brush tool with an adjustable width parameter in the 2D axial slices.

3 Results

3.1 White Matter Segmentation

We performed WM segmentation on synthetic MRI brain phantoms generated from the BrainWeb Simulated Brain Database [1,3]. The BrainWeb phantoms are available with a variety of realistic noise characteristics and the ground truth classification of each voxel is known. We tested on six noise levels (SNR = ∞, 100, 33, 20, 14, 11) with 0% RF inhomogeneity, used eight sets of seed points, and sixteen α values ranging from 0 to 0.30 (step-size of 0.02). RF inhomogeneity was not varied due to the availability of effective approaches to bias correction [15]. The eight sets of seed points were placed by 3 independent users and saved for repeated measurements. In total 768 WM segmentations were performed (6 SNR levels x 8 sets of seed regions x 16 α values). For each segmentation, accuracy was evaluated relative to the BrainWeb classification (truth) by computing

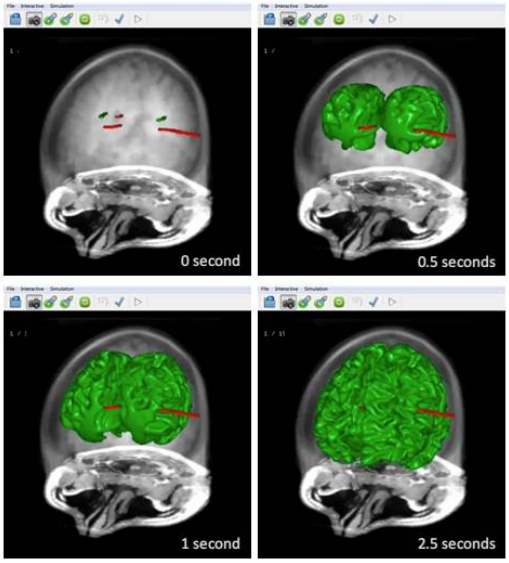

Fig. 1. The 3D view of level set propogation in BrainWeb data (SNR = 33 and RF = 0%). The overall accuracy (Dice coefficient) of level set segmentation of white matter across the entire brain was 97%. The GPU level set (including kNN computation) required 3s to execute. Total segmentation time, inlcuding data loading and user interaction, was 20s.

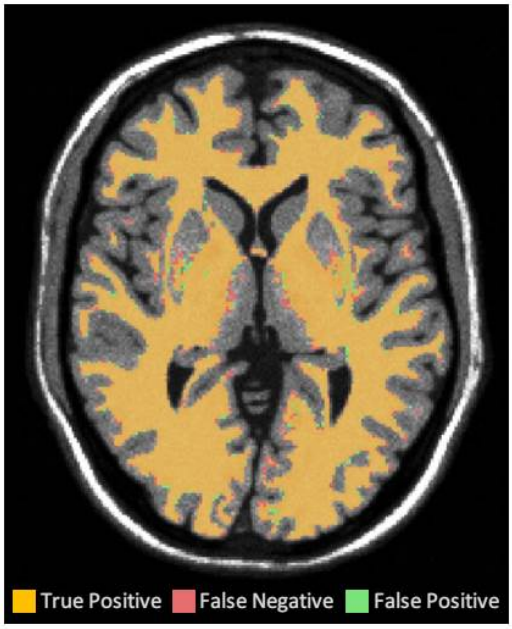

Fig. 2. The difference between our level set segmentation and Brainweb ground truth, in the axial slice with the greatest number of errors.

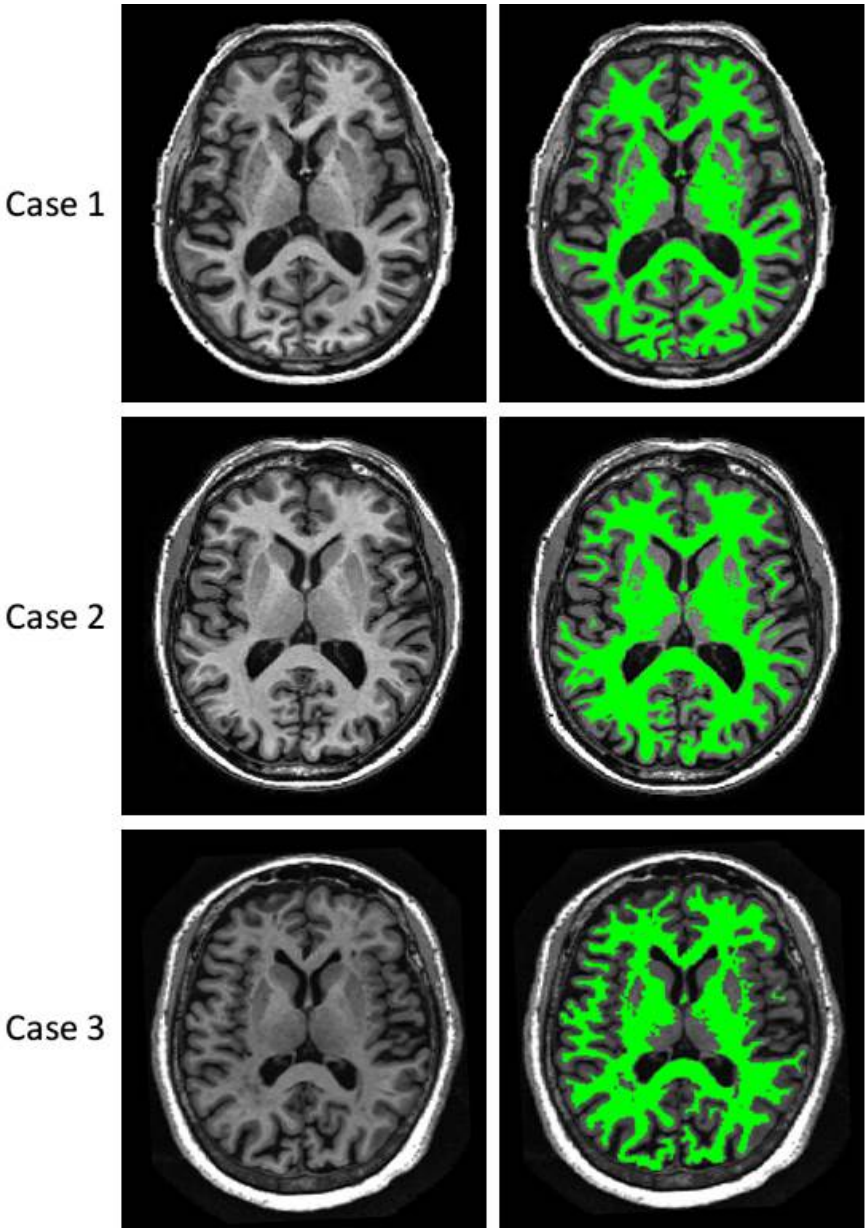

Fig. 3. Level set results on patient images. The figures in the left column show the axial slices (selected to be at a location similar to Fig. 2. The right column shows the segmentation results obtained using our method.

Dice's coefficient (Dice), a measure of spatial overlap ranging from 0 to 1, with 1 indicating perfect overlap.

3.2 Optimized curvature term: α

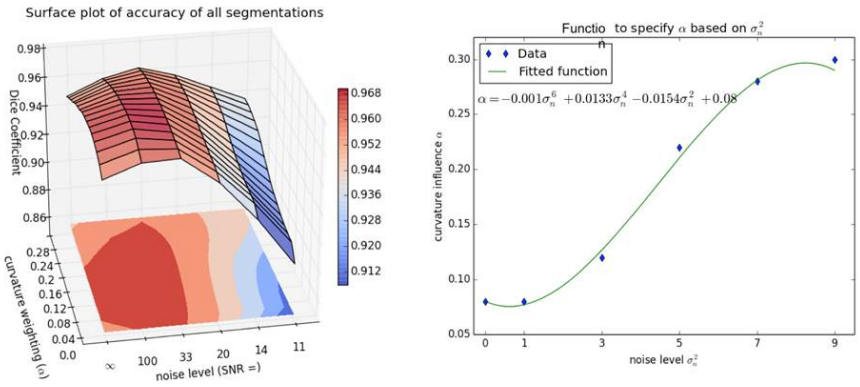

Fig. 4. The relationship between accuracy, SNR, and α for 768 WM segmentations of BrainWeb T1-weighted MR phantoms. A surface plot (left), shows the mean Dice's coefficient (accuracy) (z-axis) for different SNR values (x-axis) and curvature parameters (y-axis). We then fit a function along the path of peak accuracy in this surface. The resulting 3rd order polynomial (right) allows us to estimate the α value that maximizes accuracy for a particular image noise level σ_n^2.

Plotting the Dice's coefficient for each of the segmentation experiments described above allowed us to establish an empirical relationship between the image noise, α, and accuracy (Figure 4). Using this relationship, the initial curvature weight, α_{init}, can be selected (based on estimates of image noise) according to a third degree polynomial (determined by a curve fitting algorithm):

$$\alpha_{init} = f(\sigma_n^2) = -0.001(\sigma_n^2)^3 + 0.0133(\sigma_n^2)^2 - 0.0154\sigma_n^2 + 0.08 \qquad (8)$$

For clinical data with unknown noise, the estimated noise variance, $\sigma_n^2 = 1/\text{SNR}$, can be computed using the fast noise estimation method proposed by Immerker [9]. The curvature parameter can then be initialized using Eq. 8 without any user experience or intuition (users are still able to tune α afterward).

Over the range of image noise levels evaluated, the value for α (taken from the discrete subset tested) corresponding to the average (over the eight seed point sets) of the peak Dice coefficients varied considerably (Table 1). In contrast, the optimal α for each seed point set in a fixed noise level varied much less and the fine-tuning of α from the noise-based initial value to the experimentally-defined optimal α had limited impact on the accuracy (Table 2).

Table 1. The maximum Dice and corresponding α for each SNR value tested. The optimal α values range from 0.08 to 0.3.

SNR	100	33	20	14	11
Max. Dice	0.9712	0.9674	0.9550	0.9419	0.9310
α	0.08	0.12	0.22	0.28	0.3

Table 2. The maximum Dice and corresponding α for each set of input seed points when SNR=33. For comparison, the accuracy for fixed $\alpha = 0.12$ is also provided.

User	1	2	3	4	5	6	7	8
Max. Dice	0.9669	0.9683	0.9682	0.9679	0.9683	0.9671	0.9664	0.9657
α	0.06	0.10	0.12	0.12	0.12	0.14	0.12	0.14
Dice ($\alpha = 0.12$)	0.9668	0.9683	0.9682	0.9679	0.9683	0.9671	0.9664	0.9656

4 Discussion

Requiring users to adjust parameters increases segmentation variability, and inconvenience. Iterative refinement of parameters may also increase segmentation time. In general, the tuning process requires expertise and hinders use in clinical settings. Our new approach provides precise, accurate, rapid and simple WM segmentation in T1-weighted brain MR scans. It does not require prior knowledge of appropriate parameter values, nor extensive parameter tuning to obtain acceptabale results. We accomplished this through three novel contributions: 1) a GPU level set speed function driven by a non-parametric k-NN data model built from the seed ROI intensities; 2) a new empirical relationship between WM segmentation accuracy, image noise, and the level set curvature parameter, α; and, 3) a GPU implementation where both the level set and visualization algorithms share data buffers. This allows interactive tuning of algorithm parameters along with real-time 2D or 3D visualization of the parameter effects on segmentation results.

Future efforts will focus on validating our method for WM segmentation in other imaging modalities, such as T2-weighted MRI. We will also extend the method for segmentation of brain gray matter and ventricles.

5 Supplementary material

We have used our tool to segment a variety of objects from MR and CT datasets. A video of our tool segmentating brain WM (from T1-weighted MRI) and brain vasculature (from contrast enhanced CT) is available here: `http://goo.gl/2K98Gs`.

References

1. BrainWeb: Simulated Brain Database, `http://www.bic.mni.mcgill.ca/brainweb/`

2. Brinkley, J.F., Rosse, C.: Imaging and the Human Brain Project: a review. Methods of information in medicine 41, 245–260 (2002)
3. Collins, D.L., Zijdenbos, A.P., Kollokian, V., Sled, J.G., Kabani, N.J., Holmes, C.J., Evans, A.C.: Design and construction of a realistic digital brain phantom. IEEE transactions on medical imaging 17(3), 463–8 (Jun 1998)
4. Dang, M., Modi, J., Roberts, M., Chan, C., Mitchell, J.R.: Validation study of a fast, accurate, and precise brain tumor volume measurement. Computer methods and programs in biomedicine 111(2), 480–7 (Aug 2013)
5. Duda, R.O., Hart, P.E., Stork, D.G.: Pattern Classification (2nd Edition). Wiley-Interscience (2000)
6. Ge, Y., Grossman, R.I., Babb, J.S., Rabin, M.L., Mannon, L.J., Kolson, D.L.: Age-Related Total Gray Matter and White Matter Changes in Normal Adult Brain. Part I: Volumetric MR Imaging Analysis. Am. J. Neuroradiol. 23(8), 1327–1333 (Sep 2002)
7. Giedd, J.N., Blumenthal, J., Jeffries, N.O., Castellanos, F.X., Liu, H., Zijdenbos, A., Paus, T., Evans, A.C., Rapoport, J.L.: Brain development during childhood and adolescence: a longitudinal MRI study. Nature neuroscience 2(10), 861–3 (Oct 1999)
8. Hirono, N., Kitagaki, H., Kazui, H., Hashimoto, M., Mori, E.: Impact of White Matter Changes on Clinical Manifestation of Alzheimer's Disease : A Quantitative Study. Stroke 31(9), 2182–2188 (Sep 2000)
9. Immerkæ r, J.: Fast Noise Variance Estimation. Computer Vision and Image Understanding 64, 300–302 (1996)
10. Lefohn, A.E., Cates, J.E., Whitaker, R.T.: Interactive , GPU-Based Level Sets for 3D Segmentation. LNCS 2878 Proc MICCAI pp. 564–572 (2003)
11. Osher, S., Fedkiw, R.P.: Level set methods: An overview and some recent results. Journal of Computational Physics 169(2), 463 – 502 (2001)
12. Roberts, M., Packer, J., Sousa, M.C., Mitchell, J.R.: A work-efficient GPU algorithm for level set segmentation. In: Proc of the Conference on High Performance Graphics. pp. 123–132 (2010)
13. Sanfilipo, M.P., Benedict, R.H.B., Weinstock-Guttman, B., Bakshi, R.: Gray and white matter brain atrophy and neuropsychological impairment in multiple sclerosis. Neurology 66(5), 685–92 (Mar 2006)
14. Sethian, J.A.: Level set methods and fast marching methods (1999)
15. Tsang, O., Gholipour, A., Kehtarnavaz, N., Gopinath, K., Briggs, R., Panahi, I.: Comparison of tissue segmentation algorithms in neuroimage analysis software tools. Conference proceedings : Annual International Conference of the IEEE Engineering in Medicine and Biology Society. IEEE Engineering in Medicine and Biology Society. Conference 2008, 3924–3928 (2008)
16. Yushkevich, P.a., Piven, J., Hazlett, H.C., Smith, R.G., Ho, S., Gee, J.C., Gerig, G.: User-guided 3D active contour segmentation of anatomical structures: significantly improved efficiency and reliability. NeuroImage 31(3), 1116–28 (Jul 2006)